Commun. Theor. Phys. **68** (2017) 678–686 Vol. 68, No. 5, November 1, 2017

Structural and Mechanical Properties of TiN-TiC-TiO System: First Principle Study*

Ali Reza Farhadizadeh,[1] Ahmad Ali Amadeh,[1,†] and Hamidreza Ghomi[2]

[1]School of Metallurgy and Materials Engineering, College of Engineering, University of Tehran, P.O. Box 11155-4563, Tehran, Iran

[2]Laser and Plasma Research Institute, Shahid Beheshti University, Evin. P.O. Box 1983963113, Tehran, Iran

(Received June 7, 2017; revised manuscript received July 25, 2017)

Abstract *Mechanical and structural properties of ternary system of TiN-TiO-TiC are investigated using first principle methods. 70 different compositions of $Ti_{100}(NOC)_{100}$ with cubic structure are examined in order to illustrate the trend of properties variations. The geometry of compounds is optimized, and then, their chemical stability is assessed. Afterward, shear, bulk and young moduli, Cauchy pressure, Zener ratio, hardness and H^3/E^2 ratio are computed based on elastic constants. Graphical ternary diagram is used to represent the trend of such properties when the content of nitrogen, oxygen and carbon varies. The results show that incorporation of oxygen into the system decreases the hardness and H^3/E^2 ratio while subsequently ductility increases due to positive Cauchy pressure. It is revealed that the maximum H^3/E^2 ratio occurs when both nitrogen and carbon with a little amount of oxygen are incorporated. $Ti_{100}N_{30}C_{70}$ owns the highest hardness and H^3/E^2 ratio equal to 39.5 and 0.2 GPa, respectively. In addition, the G/B of this compound, which is about 0.9, shows it is brittle. It is also observed that the solid solutions have better mechanical properties with respect to titanium nitride and titanium carbide. The obtained results could be used to enhance monolayer coatings as well as to design multilayers with specific mechanical properties.*

PACS numbers: 62.20.Dc, 62.20.-x, 17.15.Mb **DOI:** 10.1088/0253-6102/68/5/678
Key words: mechanical properties, structural properties, first principles calculation, elastic constant

1 Introduction

In recent years, the application of hard ceramic thin films deposited by various methods of physical vapor deposition (PVD) and chemical vapor deposition (CVD) such as magnetron sputtering (MS), cathodic arc PVD, plasma enhanced CVD (PECVD) etc. has been widely extended.[1−3] Many industries including aerospace, oil and refinery, the military are using different engineered thin films deposited by vacuum methods to increase the components lifetime.[4−5] Huge studies have already been carried out to develop coatings with better wear,[6−8] solid particle erosion (SPE)[9] and corrosion resistance.[10] Furthermore, nano multilayer systems and alloying the hard compounds such as TiN, TiC, with other elements like aluminum, chromium, silicon have found a lot of interest to increase the durability of the coatings in different environments.[10−14] Because of the typical method used for depositing like reactive DC magnetron sputtering or chemical vapor deposition, the chemical composition of the coatings could be quite variable[15] in which the properties of the non-stoichiometry or solid solution deposited films are not fully documented in the literature. Furthermore, because of industrial applications of titanium nitride, titanium carbide, titanium carbonitrides and titanium oxynitride coatings, theoretical[16−19] or experimental[20−22] studies have been extensively conducted but mainly on TiN, TiC, binary systems of TiN-TiC,[23−29] TiC-TiO,[30−31] TiN-TiO[32] and there is little knowledge about the ternary system of TiN-TiC-TiO. For instance, Jiang *et al.*[33] studied deeply the structural properties of binary systems of TiN-TiO, TiN-TiC, and TiC-TiO, and showed when the oxygen content exceeds 80 at %, the experimental measurements of interplaner spacing deviates from theoretical calculations. However, the effect of simultaneous incorporation of nitrogen, oxygen, and carbon was not studied. Elastic properties of $TiN_xC_yO_{1-x-y}$ alloys are of prominence to estimate their mechanical behavior. For ternary TiN-TiC-TiO compounds, the values of bulk modulus B, shear modulus G Young modulus E, Poisson Ratio, and elastic constant of single crystals C_{ij} are only documented for TiN, TiC, TiO and some $TiN_xC_yO_{1-x-y}$ compounds, even though the data, to some extent, are scattered.[34−37] In addition, to our current knowledge, the optimal mechanical properties of titanium oxycarbonitrides have not been investigated. Furthermore, owing to a multilayer coating design, it seems essential to know the properties of every single layer deposited on the substrate in which the properties of the coating system are further predictable. The present paper aims to study the chemical and mechanical stability, structural and elastic properties, hardness and H^3/E^2 ratio (wear resistance) of $TiN_xC_yO_{1-x-y}$ compounds in the

*The authors would like to acknowledge the financial support of University of Tehran Science and Technology Park for this research under Grant No. 94061

†Corresponding author, E-mail: amadeh@ut.ac.ir

whole compositional range ($0 \leqslant x \leqslant 1$, $0 \leqslant y \leqslant 1$) by first principle method in order to offer the best titanium oxycarbonitrides composition for the coatings in terms of hardness and wear resistance. Finally, the electronic properties of TiN, TiO and TiC were also investigated to shed further light on their mechanical behavior.

2 Computational Methodology

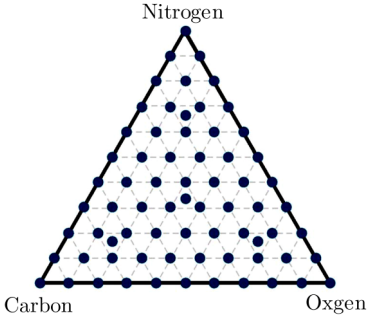

Fig. 1 Simplex design plot of $Ti_{100}(N_xO_yC_z)_{100}$ in ternary diagram where 70 compounds (solid circles) selected to investigate the properties.

First principle calculations on the ternary system of TiN-TiO-TiC were carried out with the CASTEP[38] code based on density functional theory (DFT) implemented in Material Studio Software. The models were built using Virtual Crystal Approximation (VCA) method in which it allows to perform calculation on disordered system. Local density approximation (LDA-CA-PZ)[39] and generalized gradient approximation (GGA) with specific functional including PBE,[40] RPBE,[41] PW91,[42] WC,[43] and PBESOL[44] were applied to the phases for which the properties are already known such as TiN, TiC, and pure titanium to determine the best functional for use on other compounds in the mentioned range. For geometry optimization, the quality was set to ultrafine where the convergence thresholds for energy and maximum force were 5×10^{-6} eV/atom and 0.01 eV/A, respectively. In addition, the minimization process was performed within BFGS algorithm.[45] The simplex design plot as it is depicted in Fig. 1 was used to investigate the influence of each element on structural and mechanical properties. As shown in this figure, axial and center points were also implemented to modify the design in order to gain a better insight of what happens in the design.

3 Results and Discussion

3.1 *Functional Evaluation*

To determine the most accurate functional to predict the lattice constant, stoichiometric titanium nitride, titanium carbide and pure titanium were assessed by different DFT exchange-correlation potential and the results are listed in Table 1. As it is presented, the methods with the least error for titanium nitride are GGA-PW91 and GGA-PBE, for titanium carbide is GGA-PW91, and for titanium are GGA-PW91 and GGA-PBE. Both exchange-correlation potential GGA-PW91 and GGA-PBE are appropriate to be performed for prediction of lattice constant of stoichiometric TiN, TiC, and pure titanium. However, in this study, only GGA-PW91 was employed and it might be the best available tool to predict the lattice constant of $TiN_xC_yO_{1-x-y}$. Afterward, the elastic and electronic properties were also investigated by GGA-PW91. Furthermore, based on Jiang *et al.*[33] it was found that for TiN_xO_{1-x} and TiC_xO_{1-x}, when the percentage of oxygen becomes more than 80, if the crystallographic structure remains rock salt, experimental work does not match correctly by theoretical works due to the formation of many vacancies in TiO whereas for TiN_xC_{1-x}, the theoretical data are in excellent agreement with the experimental ones.

Table 1 The calculated lattice constants of TiN, TiC, and titanium using different methods of DFT.

	TiN /Å		TiC/Å		Ti/Å	
Experimental	$a = 4.242$[46]	Error	$a = 4.327$[47]	Error	$a = 2.951$[48] $b = 4.683$[48]	Error
LDA-CA-PZ	4.175	$\%-1.6$	4.264	$\%-1.5$	$a = 2.868,\ b = 4.528$	$\%-2.8,\ \%-3.3$
GGA-PBE	4.248	%0.1	4.335	%0.2	$a = 2.945,\ b = 4.636$	$\%-0.2,\ \%-1.0$
GGA-RPBE	4.271	%0.7	4.335	$\%-0.6$	$a = 2.972,\ b = 4.679$	$\%0.7,\ \%-0.1$
GGA-PW91	4.247	%0.1	4.333	$\%-0.1$	$a = 2.933,\ b = 4.631$	$\%-0.6,\ \%-1.0$
GGA-WC	4.213	$\%-0.7$	4.303	$\%-0.5$	$a = 2.908,\ b = 4.581$	$\%-1.4,\ \%-2.2$
GGA-PBESOL	4.201	$\%-1.0$	4.299	$\%-0.6$	$a = 2907,\ b = 4.579$	$\%-1.4,\ \%-2.2$

3.2 *Structural Properties*

The crystallographic structure of titanium oxycarbonitrides is rock salt (Fig. 2). In order to perform the calculation on solid solution titanium oxycarbonitrides, atom occupancy of nitrogen, carbon and oxygen changes (blue sphere in Fig. 2) in each run. Then, the geometry optimization was carried out to reach the minimum energy and pressure. Then, we studied the chemical and mechanical stability as follows.

3.2.1 *Chemical Stability*

Chemical stability of rock salt titanium oxycarbonitrides could be investigated through cohesive energy and enthalpy of formation,[49] which are calculated as the fol-

lowing equations:[50]

$$E_{\rm coh} = \frac{E_{tot} - \sum N_i E_i^{\rm atom}}{\sum N_i}\,, \tag{1}$$

$$\Delta H_f = \frac{E_{\rm tot} - \sum N_i E_i^{\rm solid}}{\sum N_i}\,, \tag{2}$$

where $E_{\rm coh}$ is the cohesive energy, ΔH_f is the enthalpy of formation, $E_{\rm tot}$ is the total energy of the unit cell, N_i is the number of i atom in the unit cell, $E^i_{\rm atom}$ is the energies of the isolated i atom and $E^i_{\rm atom}$ denotes the total energy per atom of pure element in its ground state. Because cohesive energy is related to binding force between the atoms of a solid, it shows the chemical stability of a structure. The more negative cohesive energy is, the more stable the compound is, so it provides the information about which phase is more favorable to be formed.[51−52] During deposition of TiNCO by means of a reactive magnetron sputtering, where different gasses are purged into the chamber, cohesive energy and enthalpy of formation could be used to predict the formation of some phases in which negative enthalpy of formation and cohesive energy mean exothermic process and chemically stable structure, respectively. These energies, which is calculated in this work for $TiN_xC_yO_{1-x-y}$, show negative cohesive energy for TiN, TiC, and TiO equal to −9.38 eV, −8.94 eV, and −8.66 eV, respectively as well as negative formation enthalpy. As it is illustrated in Fig. 3(a), TiN_xO_{1-x} has negative cohesive energy and formation enthalpy for any x, implies not only it is easily formed during deposition but also it possesses strong chemical bond. Figure 3(b) presents that TiC_xO_{1-x} is not as stable as TiN_xO_{1-x}, especially when $0.2 < x < 0.8$, which the cohesive energy is positive, reaches to maximum 4.24 eV for $TiC_{0.5}O_{0.5}$. Furthermore, for any x except for 0 and 1, ΔH_f is positive which shows certain endothermic formation process. Figure 3(c), represents that TiN_xC_{1-x} has negative cohesive energy in entire range of x, although, ΔH_f for $0.1 < x < 0.6$, is small positive. Ternary map of these energies are also plotted (Fig. 4), showing that the red region, which is carbon and oxygen rich, has the most positive cohesive energy and ΔH_f. In other words, if the goal is to deposit or synthesize carbon and oxygen rich compound, there would be some difficulties owing to positive cohesive energy and formation enthalpy.

3.2.2 *Mechanical Stability*

Mechanical stability of a structure is defined by elastic constants. For cubic structure, only three of them are independent, C_{11}, C_{12}, and C_{44}, which would be discussed in details in following parts. If elastic constants of a cubic structure are satisfied in the following equations, it proves that the phases are mechanically stable.[53]

$$C_{11} > 0, \quad C_{44} > 0, \quad C_{11} > |C_{12}|\,,$$
$$(C_{11} + 2C_{12}) > 0\,. \tag{3}$$

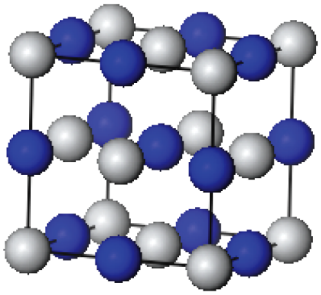

Fig. 2 The crystal structure of $Ti_{100}(N_xO_yC_z)_{100}$ where gray sphere indicates titanium and blue sphere shows nitrogen, carbon or oxygen.

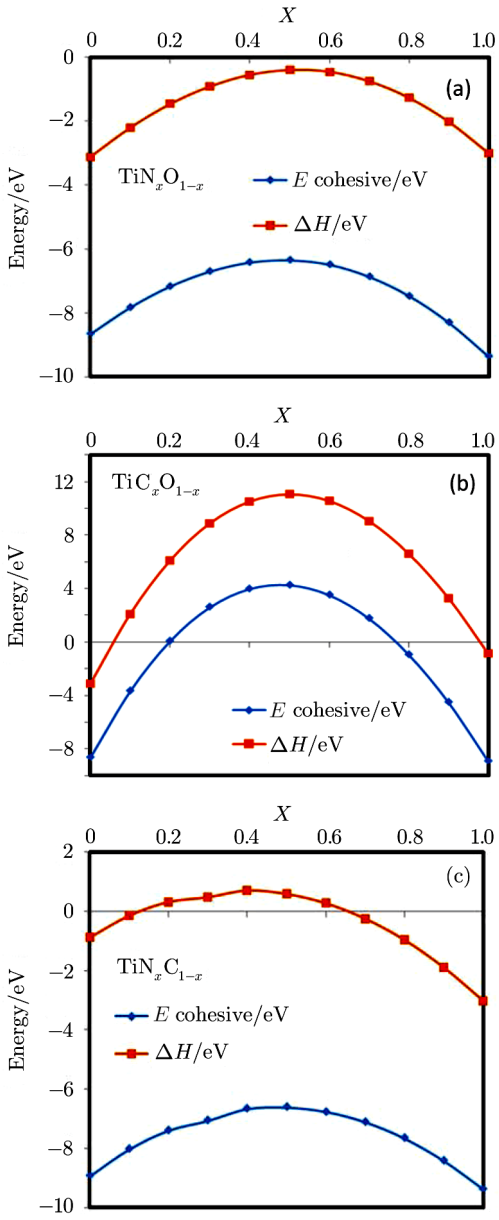

Fig. 3 The cohesive energy and formation enthalpy for (a) TiN_xO_{1-x}, (b) TiC_xO_{1-x}, and (c) TiN_xC_{1-x}.

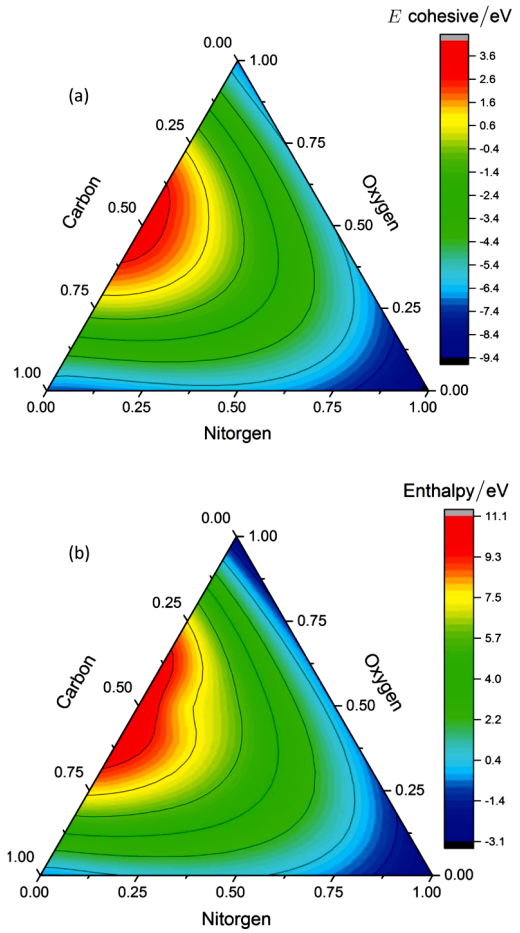

Fig. 4 Ternary map of (a) cohesive energy and (b) formation enthalpy for $Ti_{100}(N_xO_yC_z)_{100}$.

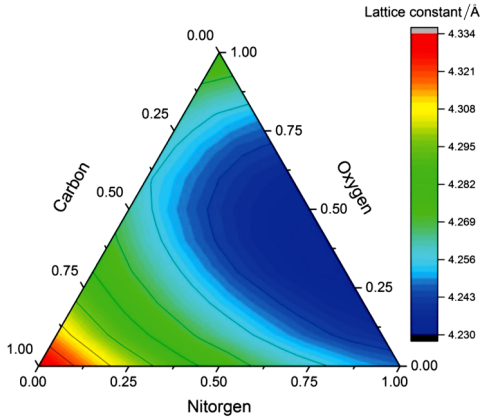

Fig. 5 Ternary map of lattice constant for $Ti_{100}(N_xO_yC_z)_{100}$.

The obtained results for 70 different compositions showed that all compounds are mechanically stable.

3.2.3 *Lattice Parameters*

It is so obvious that lattice constant alters in relation with chemical composition. In the current work, the lattice constant of $Ti_{100}(N_xO_yC_z)_{100}$ were calculated. The lattice constant changes from minimum 4.230 Å (for $Ti_{100}N_{70}O_{30}$ and $Ti_{100}N_{60}O_{40}$) to maximum 4.334 Å (for TiC) which are graphically shown in Fig. 5. This figure reveals that by adding the carbon element to TiNCO system, the lattice constant increases. At the end, it was revealed that the lattice constant does not exactly follow Vegards empirical rule[54] and the negative deviation occurs when oxygen is incorporated into the system. However, Vegards rule is quite satisfied when carbon or nitrogen content changes at a constant value of oxygen. According to Fig. 5, a given horizontal line, indicating constant oxygen content, shows a gradual increase of lattice constant approaching carbon-rich side that is in good agreement with the literature.[29]

3.3 *Mechanical Properties*

Mechanical properties of superhard materials applied as coatings are very crucial to be determined. The goal of this research is to estimate the mechanical properties including ductility, hardness, Zener ratio as well as moduli. There is a relation between mechanical properties and elastic constants. Hence, these constants are calculated at the equilibrium lattice in order to estimate the mechanical properties. Generally, there are 21 elastic constants that for cubic structure reduces to only 3 independent ones including C_{11}, C_{12}, and C_{44}.[55] Shear modulus (G) and bulk modulus (B) which shows the resistance of a material to shear deformation and shape change, respectively can be evaluated by Voigt and Reuss methods.[56] However, Hill[57] proved that Voigt and Reuss methods show the upper and lower limits of elastic constants, respectively. The Hill method represents the simple average of upper and lower bounds calculated by Voigt and Reuss method. In the following subsections the mechanical properties including ductility, hardness, yield pressure, and anisotropy ratio are thoroughly explained.

3.3.1 *Ductility*

There are some parameters associated with ductility and brittleness of materials which should be considered in details. The first is Pugh assumption[58] which predicts the toughness behavior of material by G/B ratio in which the values lower than 0.57 indicate the ductile behavior. The second one is Cauchy pressure[59] (C_{12}-C_{44}) that if it is positive, the substance is ductile. Ou *et al.*[60] stated that Poisson ratio is also a factor to evaluate the toughness of materials. In Fig. 6, the ductility of $Ti_{100}(N_xO_yC_z)_{100}$ based on Cauchy pressure, G/B ratio and Poisson ratio are shown. It is obvious that three parameters validate each other and reveals that oxygen-rich compounds are more ductile. Based on Fig. 6, it seems that brittleness is more dependent on carbon content and it consistently decreases when the carbon content increases. In principle, covalent materials with high hardness are brittle. Increasing the carbon content probably leads to stronger covalent bonding in the structure. When oxygen becomes more

than 25 percent, the red part in Fig. 6(a) disappears, indicating that ductility rises when oxygen increases.

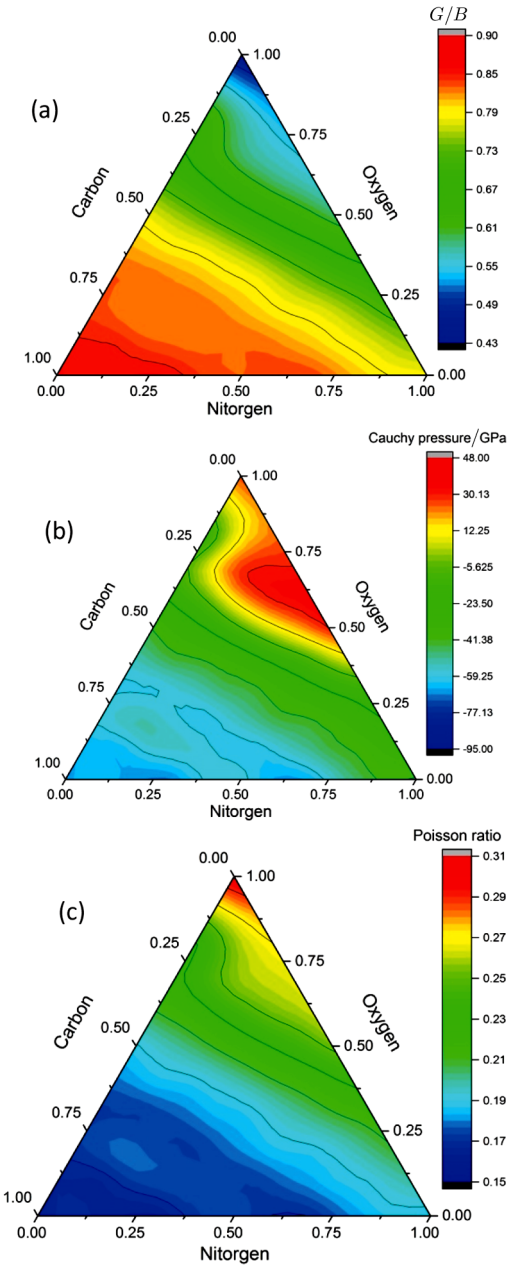

Fig. 6 The estimated ductility of $Ti_{100}(N_xO_yC_z)_{100}$ according to Pugh assumption (G/B) (a), Cauchy pressure (C_{12}-C_{44}) (b) and the Poisson ratio (c).

3.3.2 *Hardness*

It is of great prominence to calculate the hardness of novel simulated materials and it is excessively helpful to design multilayer systems. Tian *et al.*[61] proposed a semi-empirical relation to calculate the hardness of a single crystal using shear and bulk modulus as it is written below (Eq. (4)).

$$H_v = 0.92K^{1.137}G^{0.708}, \tag{4}$$

$$K = \frac{G}{B}. \tag{5}$$

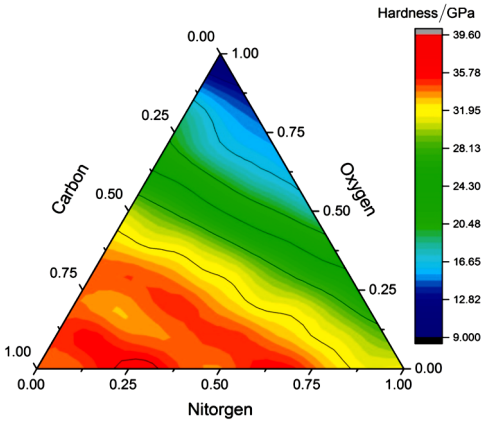

Fig. 7 The estimated hardness of $Ti_{100}(N_xO_yC_z)_{100}$.

It is stated by Lv *et al.*[62] that the hardness obtained by Eq. (4) is in good accordance with experimental measurements. In this study, the hardness was calculated and shown in Fig. 7. It is revealed that the hardest composition is $Ti_{100}N_{30}C_{70}$, which its Vickers hardness equals 39.5 Gpa and by oxygen increment, the hardness decreases to 9.1 Gpa for TiO. It is in quite agreement with other works[63−64] and shows that a large amount of oxygen incorporation lowers the hardness and mechanical properties. The hardness of titanium nitride and titanium carbide, which have much industrial application, is 32.7 Gpa and 34.5 Gpa, respectively and increases by employing both nitrogen and carbon elements. The hardness of $Ti_{100}N_{30}C_{70}$ is 15% and 20% more than TiN and TiC, respectively which is in reasonable accordance with experimental measurements.[27] Increase of hardness in solid solution $Ti_{100}N_{30}C_{70}$ can be correlated to the formation of stronger covalent and directional bonding.[61] Based on Fig. 7, when oxygen is more than 75 percent, the hardness is almost less than 15 GPa. Unlike brittleness (Fig. 6), which proportionally increased with increasing carbon, the highest hardness occurs when carbon is around 70 percent with minimum oxygen. The variation trend in Fig. 7 also implies that the hardness is more dependent on carbon content. The first ten hardest materials are listed in Table 2.

3.3.3 *Yield Pressure*

Material yield pressure is crucial for choosing the appropriate coating[8,10,65] which is often implemented to estimate the erosion and wear resistance of materials that is:

$$\text{Yield pressure} \propto \frac{H^3}{E^2}. \tag{6}$$

This relation was proposed by Ref. [66] and proved by Hassani *et al.*[65] using finite element modeling and showed that solid particle erosion resistance of different coatings can be correlated to H^3/E^2 ratio, that is, the higher H^3/E^2, the more resistance to erosion. The results are shown in Fig. 8 and it is distinctive that there

is an area near to carbon rich region (red area) that has the larger amount of H^3/E^2 ratio, containing about 15 to 30% nitrogen (x), 80 to 90% carbon (z) and 0 to 10% oxygen (y) in $Ti_{100}(N_xO_yC_z)_{100}$ leading to higher resistance to solid particle erosion. This notable finding could be used to design multilayer or monolayer hard coatings. This is also found that highest amount of this ratio, for the hardest material equals to 0.2 GPa.

Table 2 The top ten hardest materials.

	Compound	C_{11}	C_{44}	C_{12}	G	B	Vickers hardness/GPa	G/B	Zener ratio
1	$Ti_{100}N_{30}C_{70}$	563	211	116	239	265	39.5	0.90	0.94
2	$Ti_{100}N_{10}C_{80}O_{10}$	566	210	115	239	265	39.5	0.90	0.93
3	$Ti_{100}N_{50}C_{40}O_{10}$	608	197	113	238	278	37.3	0.86	0.80
4	$Ti_{100}N_{70}C_{30}$	603	196	112	237	276	37.2	0.86	0.80
5	$Ti_{100}N_{30}C_{50}O_{20}$	605	196	112	237	276	37.2	0.86	0.80
6	$Ti_{100}N_{10}C_{60}O_{30}$	598	193	111	234	273	36.7	0.86	0.79
7	$Ti_{100}N_{60}C_{40}$	578	196	122	233	274	36.2	0.85	0.86
8	$Ti_{100}N_{40}C_{50}O_{10}$	582	195	123	233	276	35.9	0.84	0.85
9	$Ti_{100}N_{20}C_{60}O_{20}$	578	194	122	231	274	35.8	0.84	0.85
10	$Ti_{100}N_{20}C_{80}$	570	191	121	223	260	35.6	0.86	0.98

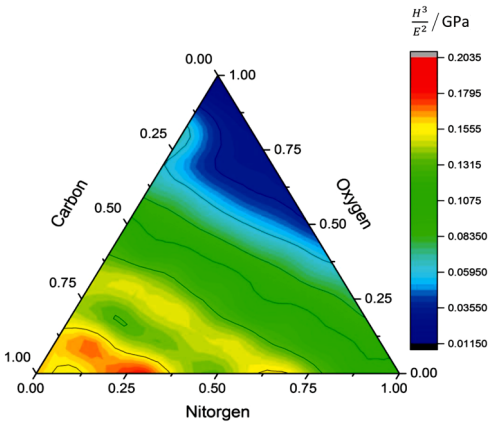

Fig. 8 The estimated H^3/E^2 of $Ti_{100}(N_xO_yC_z)_{100}$.

Table 3 The top ten materials with the highest $^3/E^2$ ratio, G/B, and Zener ratio.

	Compound	H^3/E^2 ratio	G/B	Zener ratio
1	$Ti_{100}N_{30}C_{70}$	0.20	0.90	0.94
2	$Ti_{100}N_{10}C_{80}O_{10}$	0.20	0.90	0.93
3	$Ti_{100}N_{70}C_{30}$	0.17	0.86	0.800
4	$Ti_{100}N_{30}C_{50}O_{20}$	0.17	0.86	0.80
5	$Ti_{100}N_{50}C_{40}O_{10}$	0.17	0.86	0.80
6	$Ti_{100}C_{100}$	0.17	0.86	0.92
7	$Ti_{100}N_{20}C_{80}$	0.17	0.86	0.98
8	$Ti_{100}N_{10}C_{60}O_{30}$	0.17	0.86	0.79
9	$Ti_{100}C_{90}O_{10}$	0.16	0.85	0.96
10	$Ti_{100}N_{60}C_{40}$	0.16	0.85	0.86

3.3.4 *Anisotropy Ratio*

Another important parameter is anisotropy ratio (A) or Zener ratio[55] which is a dimensionless value to quantify the anisotropy of a cubic crystal (Eq. (7)) where the value one means an ideal isotropic material. The anisotropy is a factor which represents the susceptibility to micro-cracks initiation in a material.[62] The calculated Zener ratio for hardest $Ti_{100}(N_xO_yC_z)_{100}$ is shown in Table 2. It is revealed that the least anisotropy happens in a carbon-rich system where oxygen and nitrogen are less than 25 and 50 percent, respectively. The low anisotropy, which happens in hard $Ti_{100}N_{30}C_{70}$, implies that it is probably quite durable in wear and erosion application.

$$A = \frac{2C_{44}}{C_{11} - C_{12}}\,. \tag{7}$$

3.4 *Electronic Properties*

Electronic properties play an important role to understand more about the nature of materials and specifically the mechanical properties. In the current work, the density of states (DOS), and partial density of states (PDOS), which reveals the bonding characteristics,[67] has been calculated for TiN, TiC, and TiO (Fig. 9). The Fermi level (Ef) is also depicted by the dashed line. In three phases, there are almost four regions including lower electron band, occupied by Ti-3s (−56 eV to −58 eV), middle electron band, occupied by Ti-3p (−33 eV to −35 eV), upper electron band, contributed by M-2s where M = N, O and C, and conduction unoccupied states. The upper electron band for TiN, TiO, and TiC is ranging from −18 eV to −16 eV, from −23 eV to −21 eV and from −12 eV to −9 eV, respectively. The Fermi value for TiN, TiO, and TiC are 0.76, 1.18, and 0.15 which shows the metallic behavior of these phases. The Fermi level is dominated by Ti-3d states and a small contribution of N-2p, O-2p, and C-2p for TiN, TiO, and TiC, respectively. Ti-3d electrons in three phases are delocalized from valence band to conduction band, showing the metallic nature of Ti-Ti bond. In TiC, C-2p electrons are also delocalized to some extent indicating somehow metallic bond of C-C. The p-d hybridization between N and Ti atoms (−7 eV to −2 eV)

is stronger than O and Ti (−10 eV to −5 eV), which indicates stronger Ti-N covalent bond. The p-d hybridization between C and Ti atoms (−5 eV to 5 eV) implies strong Ti-C covalent bond, leading to greater mechanical properties including elastic constants and hardness. Another parameter that unveils more about bonding feature is Mulliken method employed for charge calculation, bond length and population analysis presented in Table 4. The more population value, the stronger covalent band; indicating Ti-C has the strongest covalent bond amongst the investigated phases, which could be a good reason for higher elastic constants.[29]

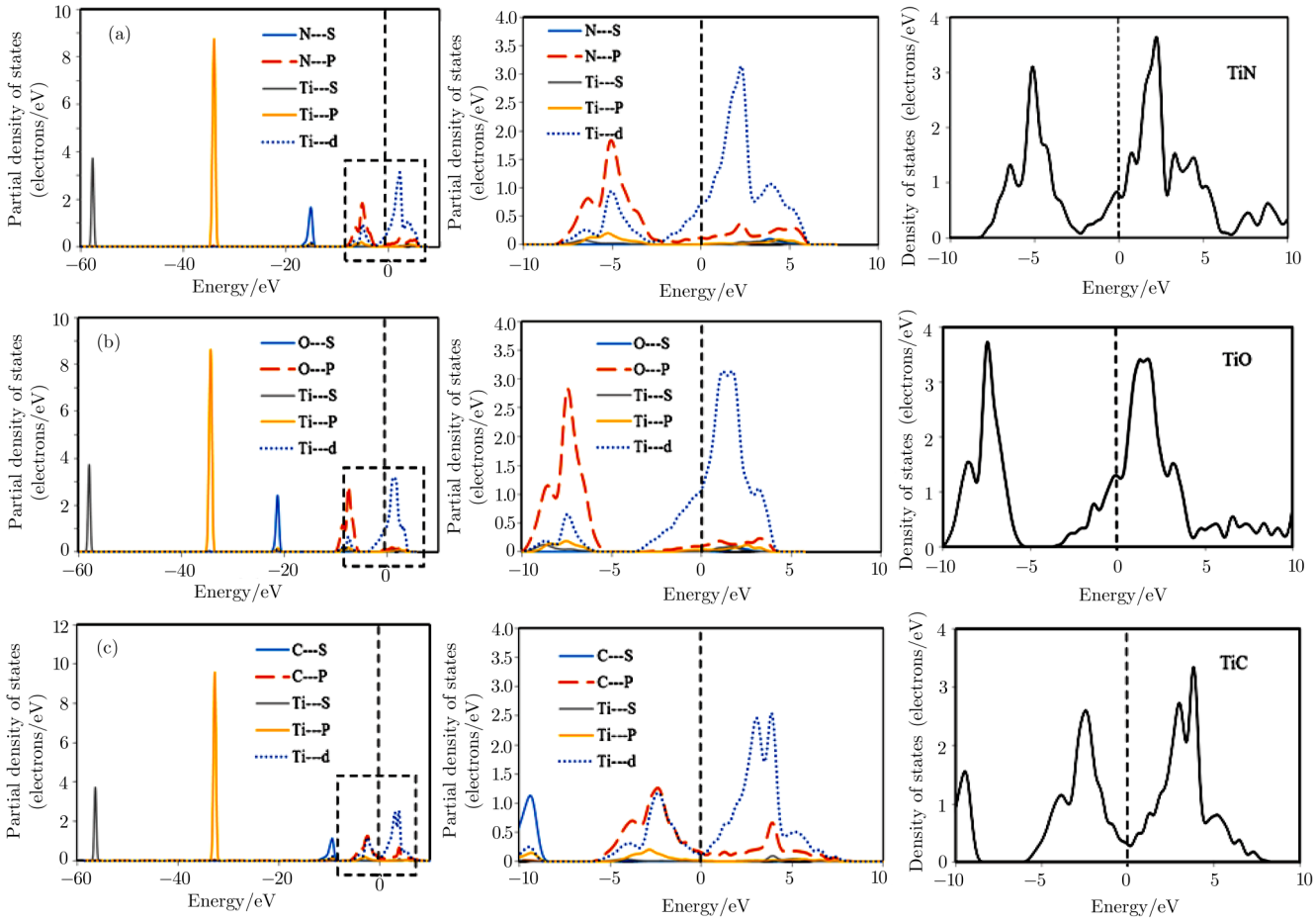

Fig. 9 Density of states and partial density of states (electrons/eV) of (a) TiN, (b) TiO and (c) TiC. The Fermi level is shown by the vertical dash line.

Table 4 Mulliken atomic population and bond length of TiN, TiC, and TiO.

Compoubd	Species	Ion	s	p	d	Total	Charge (e)	Bond	Population	Length/Å
TiN	N	1	1.68	4.85	0.00	5.74	−0.74	Ti–N	1.67	2.124
	Ti	1	12.19	6.50	2.57	11.26	0.74			
TiO	O	1	1.82	4.85	0.00	6.67	−0.67	Ti–O	1.03	2.141
	Ti	1	2.21	6.41	2.71	11.33	0.67			
TiC	C	1	1.50	3.20	0.00	4.70	−0.70	Ti–C	2.00	3.754
	Ti	1	2.13	6.58	2.59	11.30	0.70			

4 Conclusion

In this study, structural and elastic properties, hardness and H^3/E^2 ratio (wear resistance) of $TiN_xC_yO_{1-x-y}$ compounds in the whole compositional range ($0 \leqslant x \leqslant 1$, $0 \leqslant y \leqslant 1$) were calculated by DFT method using generalized gradient approximation. Chemical stability was also studied by cohesive energy and formation enthalpy. Furthermore, mechanical stability criterion was also considered, showing all phases are mechanically stable. Ternary map of lattice constant was plotted, displaying that the more carbon content, the larger lattice constant. Then, based on elastic constants, mechanical properties includ-

ing ductility, hardness, H^3/E^2 ratio and Zener ratio were calculated so as they can be used for material selection. It was shown that incorporation of oxygen, more than 15 percent, increases the ductility whereas decreases the hardness and H^3/E^2 ratio indicating that the coatings with inappropriate oxygen content do not provide improved mechanical properties. It was also found out that $Ti_{100}N_{30}C_{70}$ and $Ti_{100}N_{10}C_{80}O_{10}$ are the hardest whereas their Zener ratio is quite appropriate equal to 0.94 and 0.93. It was also revealed that suitable oxygen content (about 5 to 10 percent) as a solid solution can enhance the mechanical properties. Carbon-rich compounds are normally harder and more erosion and wear resistant materials (with higher H^3/E^2 ratio) in the investigated compositional range where their Zener ratio is near one. Although, this study only focused on some intrinsic properties of $Ti_{100}(N_xO_yC_z)_{100}$, it introduced some better material for hard coatings with the highest hardness and H^3/E^2 ratio. For further study, it is possible to investigate the non-stoichiometry $Ti_{100+t}(N_xO_yC_z)_{100-t}$ as well as the influence of layering of these compounds.

References

[1] H. E. Rebenne and D. G. Bhat, Surf. Coat. Technol. **63** (1994) 1.

[2] I. Safi, Surf. Coat. Technol. **127** (2000) 203.

[3] F. Sanchette, C. Ducros, T. Schmitt, P. Steyer, and A. Billard, Surf. Coat. Technol. **205** (2011) 5444.

[4] M. W. Reedy, T. J. Eden, J. K. Potter, and D. E. Wolfe, Surf. Coat. Technol. **206** (2011) 464.

[5] S. Muboyadzhyan, Russ. Metall. (Metally) **2009** (2009) 183.

[6] S. PalDey, S. Deevi, Mater. Sci. Eng. A **342** (2003) 58.

[7] H. N. Shah and R. Jayaganthan, J. Mater. Eng. Perfor. **21** (2012) 2002.

[8] J. Deng, F. Wu, Y. Lian, Y. Xing, and S. Li, Inter. J. Refrac. Metals Hard Mater. **35** (2012) 10.

[9] E. Bousser, L. Martinu, and J. E. Elemberg-Sapieha, Surf. Coat. Technol. **257** (2014) 165.

[10] Q. Yang, L. Zhao, F. Cai, S. Yang, and D. Teer, Surf. Coat. Technol. **202** (2008) 3886.

[11] Y. X. Xu, L. Chen, F. Pei, and Y. Du, Surf. Coat. Technol. **304** (2016) 512.

[12] E. Alat, A. T. Motta, R. J. Comstock, J. M. Partezana, and D. E. Wolfe, J. Nucl. Mater. **478** (2016) 236.

[13] J. K. Lee and G. S. Yang, Trans. Nonferrous Met. Soc. China **19** (2009) 795.

[14] V. William Grips, H. C. Barshilia, V. E. Selvi, and K. Rajam, Thin Solid Films **514** (2006) 204.

[15] J. E. Sundgren, Thin Solid Films **128** (1985) 21.

[16] H. Wang, H. Zeng, Q. Li, and J. Shen, Thin Solid Films **607** (2016) 59.

[17] D. Yin, Y. Yang, X. Peng, Y. Qin, and Z. Wang, Physica E: Low Dimens. Syst. Nanostruct. **63** (2014) 125.

[18] D. Yin, X. Peng, Y. Qin, and Z. Wang, Physica E: Low Dimens. Syst. Nanostruct. **44** (2012) 1838.

[19] V. Krasnenko and M. G. Brik, Solid State Sci. **28** (2014) 1.

[20] C. Subramanian and K. Strafford, Wear **165** (1993) 85.

[21] O. Se-Doo, K. Jong-Woo, and L. Young-Ze, Tribol. Trans. **47** (2004) 29.

[22] I. Petrov, L. Hultman, U. Helmersson, J. E. Sundgren, and J. Greene, Thin Solid Films **169** (1989) 299.

[23] H. T. Chen and M. F. Yan, Physica B: Condens. Matter **407** (2012) 1183.

[24] Y. Yang, H. Lu, C. Yu, and J. M. Chen, J. Alloys Comp. **485** (2009) 542.

[25] V. P. Zhukov, V. A. Gubanov, O. Jepsen, N. E. Christensen, and O. K. Andersen, Philos. Mag. B **58** (1998) 139.

[26] V. Richter, A. Beger, J. Drobniewski, I. Endler, and E. Wolf, Mater. Sci. Eng. A **209** (1996) 353.

[27] L. Karlsson, L. Hultman, M. Johansson, J. E. Sundgren, and H. Ljungcrantz, Surf. Coat. Technol. **126** (2000) 1.

[28] S. H. Jhi and J. Ihm, Phys. Rev. B **56** (1997) 13826.

[29] H. Chen and M. Yan, Physica B: Cond. Matter **407** (2012) 1183.

[30] A. C. Fernandes, P. Carvalho, F. Vaz, *et al.*, Thin Solid Films **515** (2006) 866.

[31] A. C. Fernandes, F. Vaz, L. Rebouta, *et al.*, Surf. Coat. Technol. **201** (2007) 5587.

[32] S. K. Rawal, A. K. Chawla, R. Jayaganthan, and R. Chandra, J. Mater. Sci. Technol. **28** (2012) 512.

[33] B. Jiang, N. Ying, Q. Wang, *et al.*, J. Am. Ceram. Soc. **97** (2014) 1288.

[34] D. Chen, J. Chen, Y. Zhao, B. Yu, C. Wang, and D. Shi, Acta Metall. Sin. (Engl.) **22** (2009) 146.

[35] J. H. Jang, C. H. Lee, Y. U. Heo, and D. W. Suh, Acta Mater. **60** (2012) 208.

[36] L. Marques, S. Carvalho, F. Vaz, *et al.*, Vacuum **83** (2009) 1240.

[37] Z. Y. Zhai, J. Peng, F. Zao, *et al.*, Physica B: Conden. Matter **405** (2010) 4620.

[38] S. J. Clark, M. D. Segall, C. J. Pickard, *et al.*, Z. Kristallog. Materials **220** (2005) 567.

[39] D. M. Ceperley and B. Alder, Phys. Rev. Lett. **45** (1980) 566.

[40] J. P. Perdew, K. Burke, and M. Ernzerhof, Phys. Rev. Lett. **77** (1996) 3865.

[41] B. Hammer, L. B. Hansen, and J. K. Nrskov, Phys. Rev. B **59** (1999) 7413.

[42] J. P. Perdew, J. Chevary, S. Vosko, *et al.*, Phys. Rev. B **46** (1992) 6671.

[43] Z. Wu and R. E. Cohen, Phys. Rev. B **73** (2006) 235116.

[44] J. P. Perdew, A. Ruzsinszky, G. I. Csonka, *et al.*, Phys. Rev. Lett. **100** (2008) 136406.

[45] B. G. Pfrommer, M. Ct, S. G. Louie, and M. L. Cohen, J. Comput. Phys. **131** (1997) 233.

[46] W. Wong-Ng, H. McMurdie, B. Paretzkin, C. Hubbard, and A. Dragoo, Powder Diffraction **2** (1987) 200.

[47] National Bureau of Standards **25** (1981) 73.

[48] R. M Wood, Proc. Phys. Soc. **80** (1962) 783.

[49] W. Yang, M. Pang, Y. Tan, and Y. Zhan, J. Phys. Chem. Solids **98** (2016) 298.

[50] Z. Zhou, X. Zhou, and K. Zhang, Computational Materials Science **113** (2016) 98.

[51] G. Abadias, V. I. Ivashchenko, L. Belliard, and P. Djemia, Acta Materialia **60** (2012) 5601.

[52] A. T. Asvini Meenaatci, R. Rajeswarapalanichamy, and K. Iyakutti, Solid State Sciences **19** (2013) 36.

[53] R. Rajeswarapalanichamy, M. Kavitha, G. Sudha Priyanga, and K. Iyakutti, J. Phys. Chem. Solids **78** (2015) 118.

[54] L. Vegard, Zeitschrift für Physik **5** (1921) 17.

[55] Z. Li and R. C. Bradt, J. Mater. Sci. **22** (1987) 2557.

[56] S. Hong and C. Fu, Intermetallics **7** (1999) 5.

[57] R. Hill, Proc. Phys. Soc. Sec. A **65** (1952) 349.

[58] P. Ravindran, L. Fast, P. A. Korzhavyi, *et al.*, J. Appl. Phys. **84** (1998) 4891.

[59] D. Pettifor, Mater. Sci. Technol. **8** (1992) 345.

[60] P. Ou, J. Wang, S. Shang, *et al.*, Surf. Coat. Technol. **264** (2015) 41.

[61] Y. Tian, B. Xu, and Z. Zhao, Inter. J. Refract. Metals Hard Mater. **33** (2012) 93.

[62] Z. Q. Lv, Z. F. Zhang, Q. Zhang, *et al.*, Solid State Sci. **56** (2016) 16.

[63] J. M. Chapp, N. Martin, J. Lintymer, *et al.*, Appl. Surf. Sci. **253** (2007) 5312.

[64] O. Banakh, M. Moussa, J. Matthey, *et al.*, Appl. Surf. Sci. **317** (2014) 986.

[65] S. Hassani, M. Bielawski, W. Beres, *et al.*, Surf. Coat. Technol. **203** (2008) 204.

[66] K. L. Johnson and K. L. Johnson, *Contact Mechanics*, Cambridge University Press, Cambridge (1987).

[67] Y. Zhao, J. Yu, L. Wu, *et al.*, Computat. Mater. Sci. **124** (2016) 273.